Compact irradiation system for evaluation of basic characteristics of the nanoDot OSL dosimeter toward direct measurement of exposure dose of patients

Poster No.:	C-0024
Congress:	ECR 2016
Type:	Scientific Exhibit
Authors:	H. Okino[1], H. Hayashi[1], K. Takegami[1], N. Kimoto[1], I. Maehata[1], Y. Kanazawa[1], T. Okazaki[2], T. HASHIZUME[3], I. Kobayashi[2]; [1]Tokushima/JP, [2]Tsukuba, Ibaraki/JP, [3]Tsukuba/JP
Keywords:	Dosimetric comparison, Dosimetry, SPECT, PET, Radioprotection / Radiation dose, Radiation physics
DOI:	10.1594/ecr2016/C-0024

Aims and objectives

Recently, patient dose management has become an important topic in the X-ray based diagnosis. This is because dose exposure has become increasingly precise during diagnosis. The relevance between the exposure dose and the quality of an obtained medical image should be managed through the measured exposure dose. In fact currently, the exposure dose is estimated by the air-kerma measurement using an ionization chamber, and the methodology to calculate the exposure dose has been established **[1-3]**. In this method, the contribution of scattered X-rays is estimated by back scatter factor (BSF) which is functions of both quality of X-ray and size of irradiation field. The problem with this method is, it does not consider the patients condition; there are large differences between patients. Therefore, we plan to measure the exposure dose directly using a dosimeter that doesn't interfere with the medical image.

Currently, a small-type OSL (optically stimulated luminescence) dosimeter, named nanoDot **[4-8]**, was commercially produced by Landauer Inc. **Figure 1** illustrates nanoDot OSL dosimeter and its reader. Our research group focuses attention on its low detection properties which enables a measurement exposure dose without interfering with the medical image **[9]**. Currently, we're studying the basic properties of the nanoDot OSL dosimeter for direct measurement of patient dose in the general X-ray region **[9-14]**. In addition, many reports have been published concerning measurements in the radiotherapeutic region **[4-6]**.

Figure 2 indicates motivation for our study. In this investigation, we focused attention on the nuclear medicine region. In this region, we should be concerned with secondary electron equilibration, because the range of secondary electrons is up to 10 m. This fact means that we should adopt an extremely large irradiation field. In reality, the maximum size of the irradiation field may be limited, also for the simulation study there is a restriction based on CPU power of the personal computer used. The aim of this study is to propose a new irradiation system, which can establish a compact irradiation field for the nuclear medicine region. Using the Monte-Carlo simulation code, we evaluated the accuracy of the proposed system.

Images for this section:

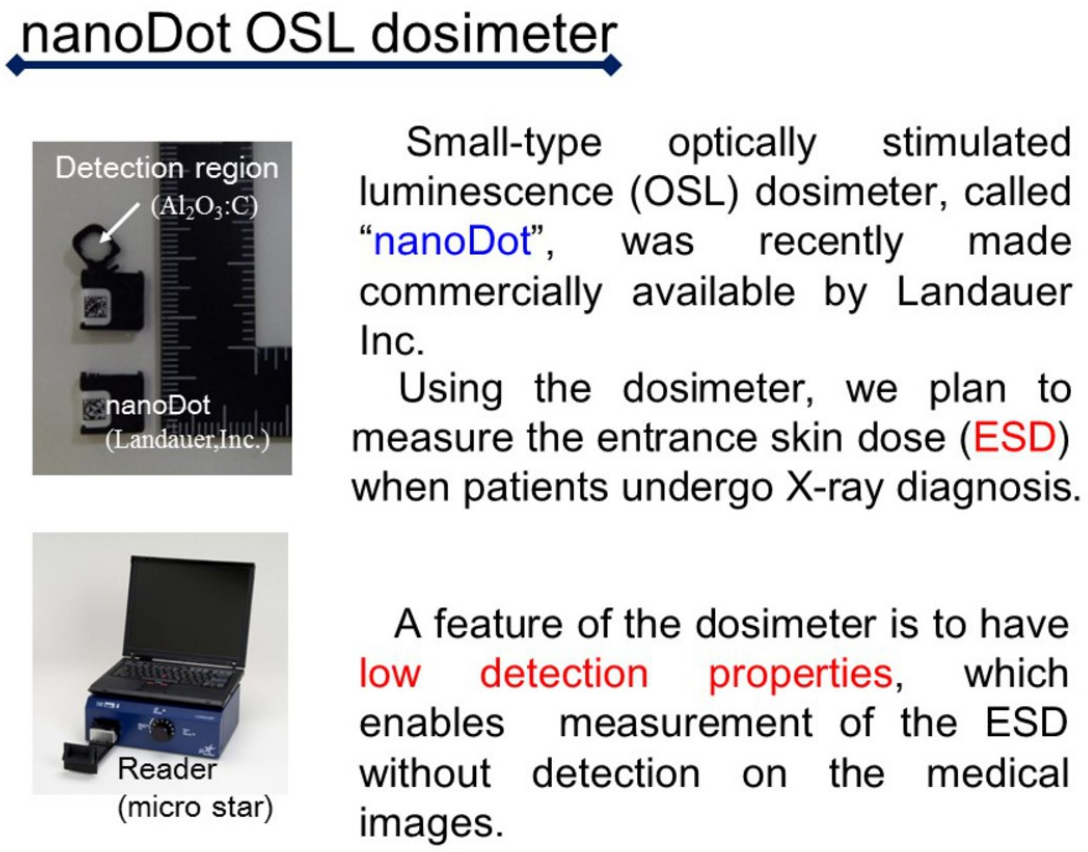

Fig. 1: Introduction of the nanoDot OSL dosimeter. NanoDot is a small-type OSL (optically stimulated luminescence) dosimeter and commercially available by Landauer Inc.

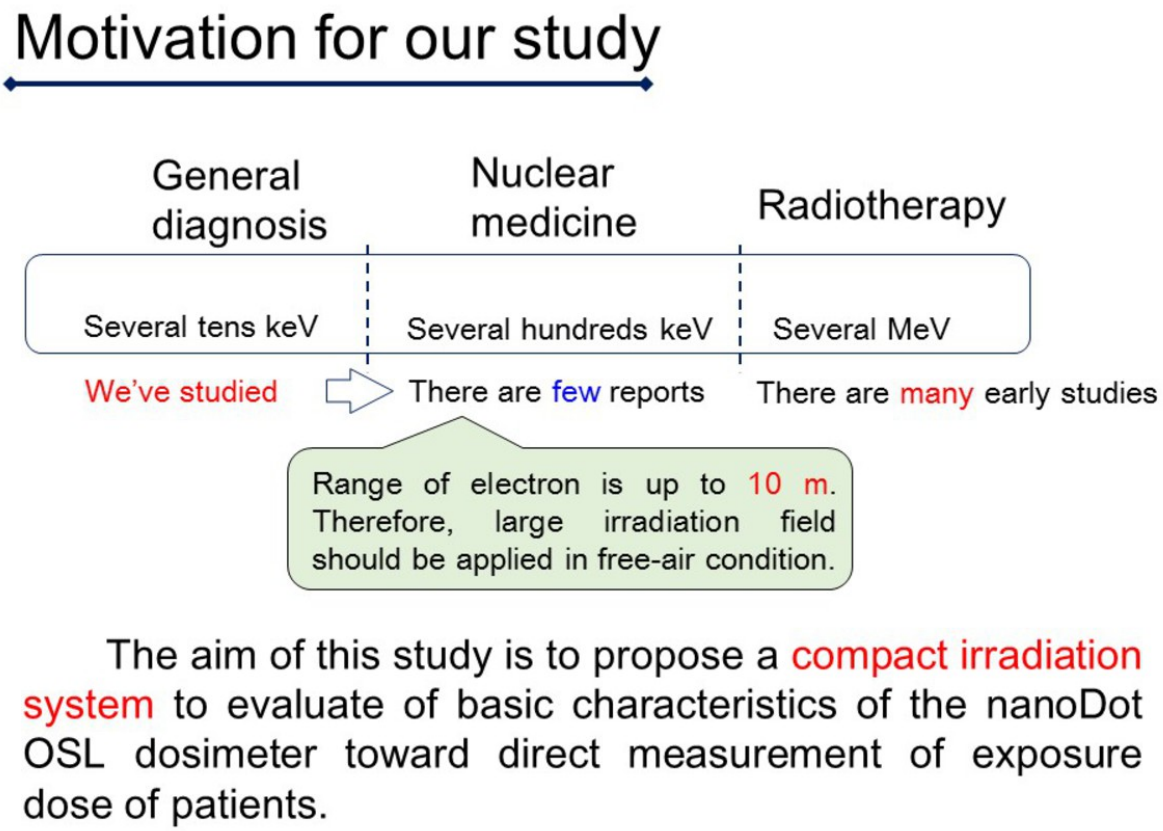

Fig. 2: The motivation for our study. Focusing attention on nuclear medicine region, we propose a new compact irradiation system for the evaluation of basic characteristics of the nanoDot OSL dosimeter.

Methods and materials

The proposed irradiation system is presented in **Fig. 3**. In order to achieve a small irradiation field, the detection region was covered with phantoms having thicknesses of "t". Here, the size of the irradiation field (S×S) was defined as S = R + 10 mm + R, where R was range of secondary electrons. **Figure 4** shows the properties of the Monte-Carlo simulation. In the present study, EGS5 (electron gamma shower ver.5) code **[15,16]** was used. The number of photons used was 10^8, the energy of photons was 100-2000 keV, and phantom thickness was from 1-15 mm. The compositions of the phantom and detection region are represented in **Fig. 4**. The detection region was filled with air or PMMA (Polymethyl methacrylate) with a density of 0.001205 g/cm^3, and the phantom region filled with air or PMMA having a density of 1.00 g/cm^3 or 1.19 g/cm^3 were applied. We then simulated the photon and electron transportations based on the following three conditions; "Air/Air" means air in the detection region and air in the phantom region, "PMMA/PMMA" means PMMA in the detection region and PMMA in the phantom region, and "Air/PMMA" means air in the detection region and PMMA in the phantom region. A detailed analysis and purpose of these materials will be described later.

The range "R" of the secondary electron field was calculated as shown in **Fig. 5**. The graph in **Fig. 5** represents energy loss of electrons as a function of electron energy **[17]**. When the electron with energy E_i penetrates the material with thickness of #t, the energy loss $\#E_i$ is calculated by $\#E_i = dE/dx(E_i)\times\#t$. Therefore, R is calculated by summation of #t until the integrated value of $\#E_i$ agrees with the incident energy of E. In this study, #t is set at 0.01 cm.

Theoretically speaking, when secondary electron equilibration is achieved, the absorbed dose D in the detection region is equal to the air-kerma K (collision kerma K_{col}). Therefore, we evaluated the consistency between D and K_{col}. A detailed description of how K_{col} is obtained from energy fluencies is presented in **Fig. 6**. Here, the reference value of the mass energy absorption coefficient is applied **[18]**.

The proposed irradiation system was simply constructed, in which the detection area was fully covered with a phantom to achieve secondary electron equilibration. Here, the thickness of the phantom is an important parameter, because the size of the irradiation field is decided by the range of secondary electrons. Then, advantages and disadvantages of our simulation were evaluated by the "efficiency of Monte-Carlo

simulation" and "fraction of scattered rays". In **Fig. 7**, these values are defined as mathematical expressions.

Images for this section:

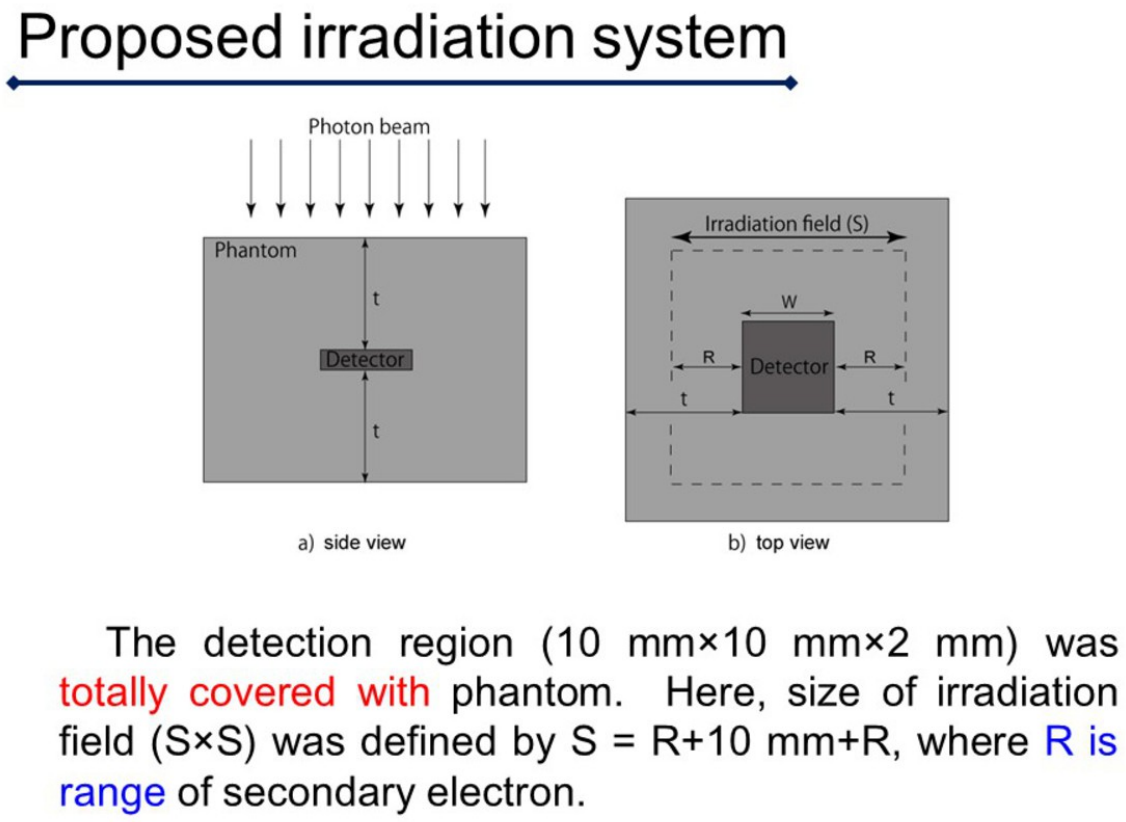

Fig. 3: The proposed irradiation system. The detection region was totally covered with phantom having variable thicknesses represented by "t".

Monte-Carlo simulation

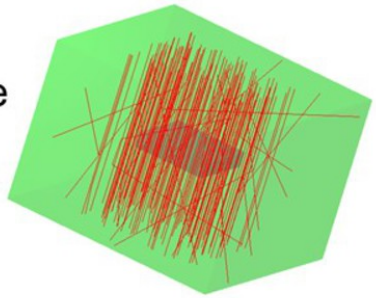

Using EGS5 (electron gamma shower ver.5) code

- Number of photon used: 10^8
- Energy of photons: 100-2000 keV
- Phantom thickness: 1, 5, 10, 15 mm

Compositions of phantom and detection region

Aim	Description	Detection region	Phantom
For check of verification at ideal condition	(Air/Air)	Air (0.001205 g/cm^3)	Air (1.00 g/cm^3)
For check of simulation accuracy	(PMMA/PMMA)	PMMA (0.001205 g/cm^3)	PMMA (1.19 g/cm^3)
For applying the realistic condition	(Air/PMMA)	Air (0.001205 g/cm^3)	PMMA (1.19 g/cm^3)

Fig. 4: Property of the Monte-Carlo simulation code. We used EGS5 (electron gamma shower ver.5) code. Details of the conditions and compositions of phantoms and detection regions are presented.

Calculation of range for electron

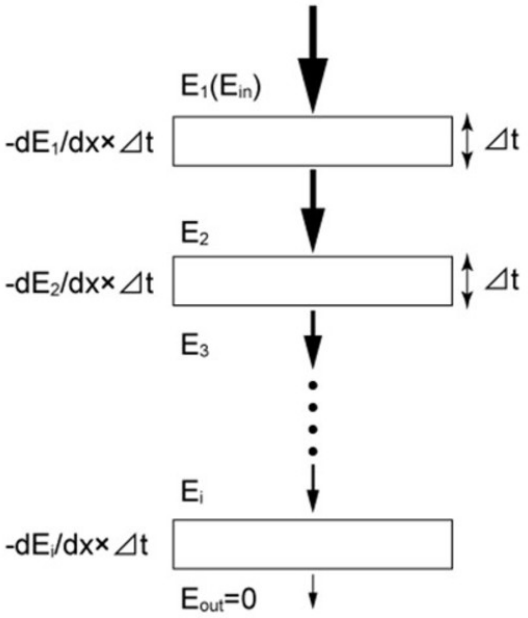

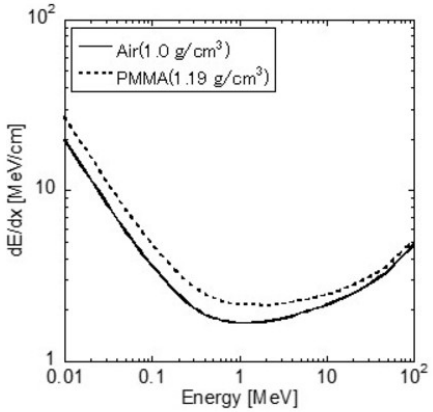

Lucien Pages, Evelyne Bertel, Henri Joffre, et al.
Energy Loss, Range, and Bremsstrahlung Yield for 10-kev to 100MeV Electrons in Various Elements and Chemical Compounds
Atomic Data and Nuclear Data Tables 4, 1-127(1972)

$$R = \sum_{i=1}^{n} \Delta t \qquad (\Delta t = 0.01 \text{ cm})$$

Fig. 5: Calculation methodology for range for secondary electron (see text).

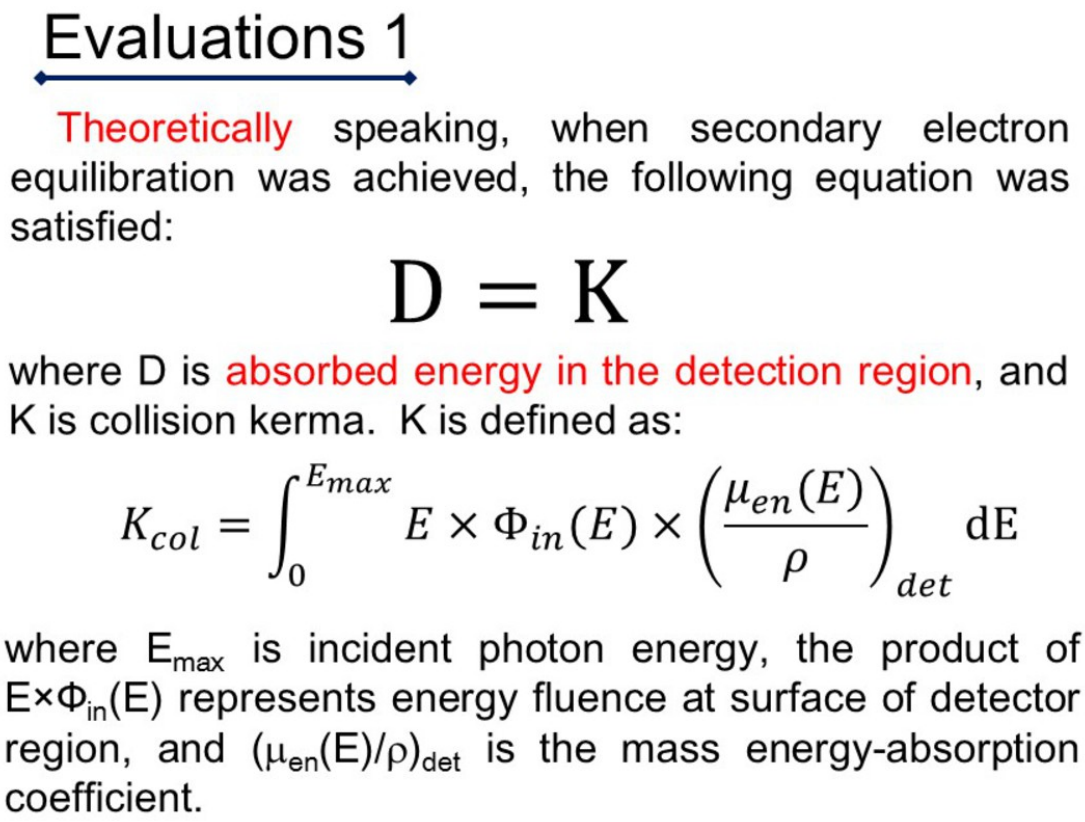

Fig. 6: Evaluation method to prove our calculation. We checked the consistency between the absorbed dose D in the detection region and the air-kerma K (collision kerma K)

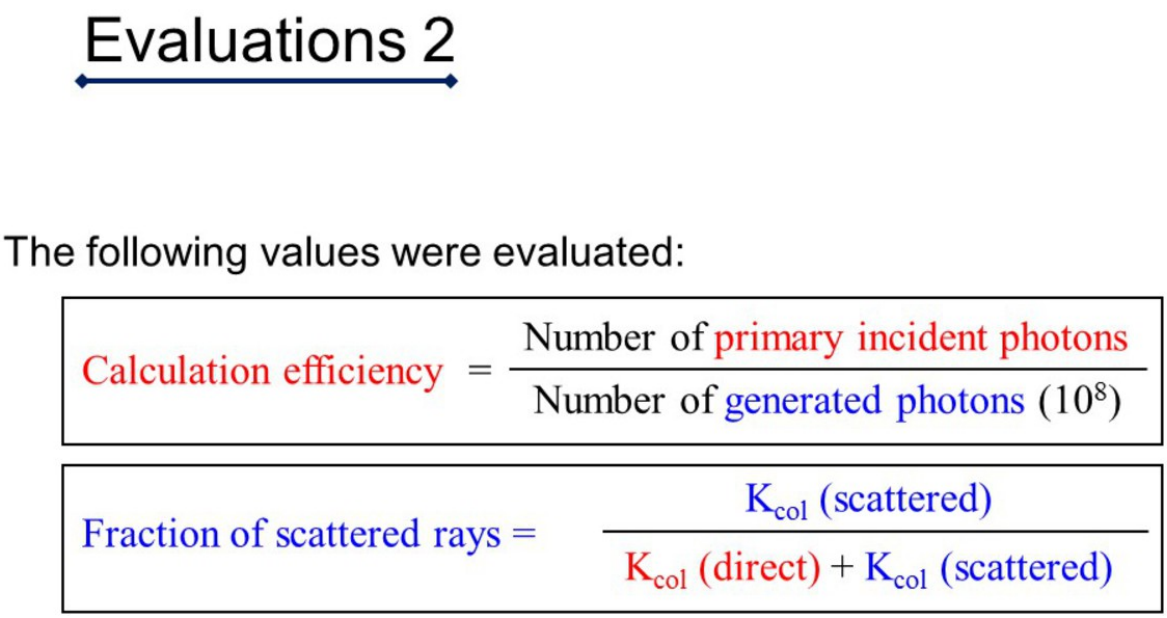

Fig. 7: The evaluation method of the proposed system. We calculated the efficiency of the Monte-Carlo simulation and fraction of scattered rays.

Results

When calculating the irradiation field, it was found that phantom thicknesses of 1 mm, 5 mm, and 10 mm were necessary to achieve electron equilibration for 100-300 keV, 400-1000 keV, and 1500-2000 keV photons, respectively.

Figure 8 shows the results of the consistency check for D and K_{col}. The vertical axis shows that D/K_{col}, so $D/K_{col}=1$ is the ideal value. The corresponding values of "Air/ Air" (blue) and "PMMA/PMMA" (green) deviate within the range of 1±0.05. On the other hand, the corresponding value of "Air/PMMA" (red) is systematically lower than 1, therefore, they are included in the range between 0.9 and 1.

Left graph in **Fig. 9** shows the calculation efficiency for the condition of "Air/PMMA" for 100-2000 keV photons. The calculation efficiency becomes 70-90% for 100 keV and approximately 10% for 2000 keV. For 100 keV photons, the calculation efficiency for 1 mm and 5 mm thicknesses are about 20% larger than those of 10 mm and 15 mm because a phantom thickness of 1 mm is sufficient for 100 keV and additional thickness results in attenuation. When increasing photon energy up to 1000 keV, the differences become small. We determined that proper phantom thickness should be applied based on photon energy.

The right graph in **Fig. 9** shows the fraction of scattered rays for the condition of "Air/ PMMA" for 100-2000 keV photons. For the 1mm thick phantom, the fraction of scattered X-rays varies approximately from 1.1% to 1.6% for photon energies from 100 keV to 300 keV. The 5 mm thick phantom varies approximately 2.7% to 4.7% for photon energies from 100 keV to 800 keV. The 10 mm thick phantom varies approximately 3.1% to 6.6% for photon energies from 100 keV to 2000 keV. Phantom thickness of 15 mm varies approximately 4.3% to 7.3% for photon energies of 100 keV to 2000 keV. As clearly seen in the graph, the thicker the phantom used, the more intense the scattered rays were generated.

Efficiency of Monte-Carlo simulation becomes 70-90% for 100 keV and approximately 10% for 2000 keV. These values are much higher than those without phantoms. Fraction

of scattered rays becomes several percentages. Moreover we estimated the accuracy of the simulation. From these results, we evaluated that the accuracy of our system is approximately 10%.

Finally, we demonstrate the ability of the proposed method. **Figure 10** shows results from an additional simulation, in which three different irradiation systems are applied; system A is the proposed system, in system B the detection region is partially covered with a phantom and sides are not covered, and in system C the detection region is not covered and the phantom is just placed in front of the detection region. The second condition is similar to the previously proposed practical experimental irradiation system which is valuable to achieve secondary electron equilibration **[19]**. The graph shows the availability of the proposed system; namely, D/K_{col} value of the proposed system (system A: red) is approximately 1, but for systems B (green) and C the systematical value is smaller. The phenomenon indicates the importance of covering the detection region completely.

Images for this section:

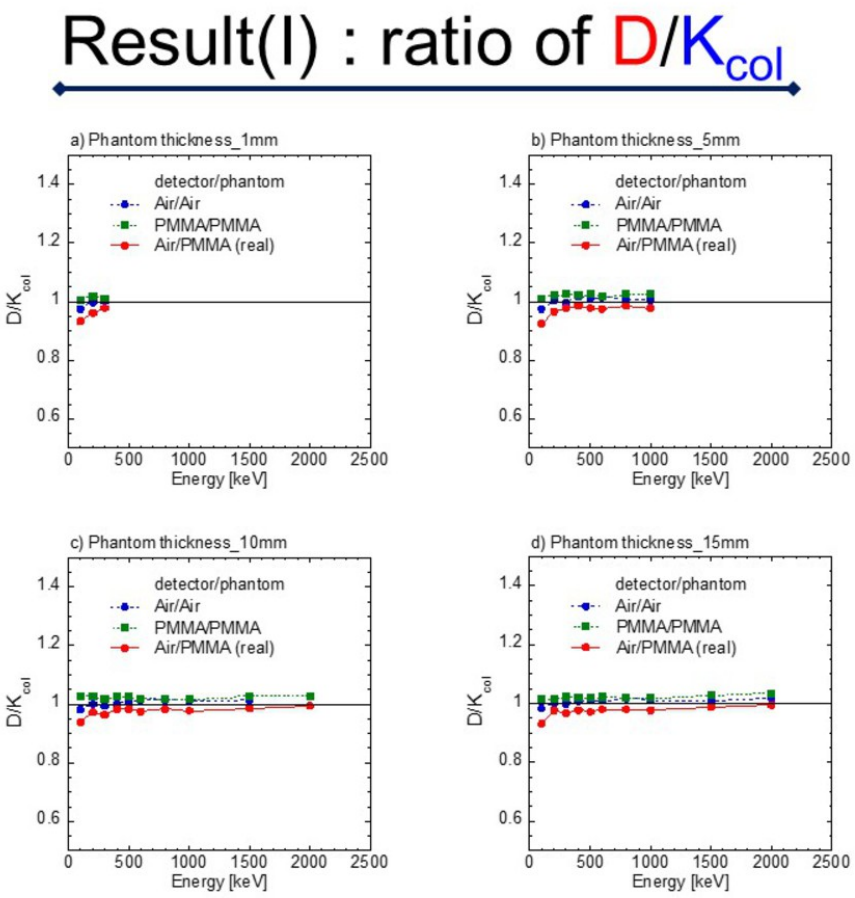

Fig. 8: Results of consistency checks of D and K.

Result(II) :

Calculation efficiency and fraction of scattered rays

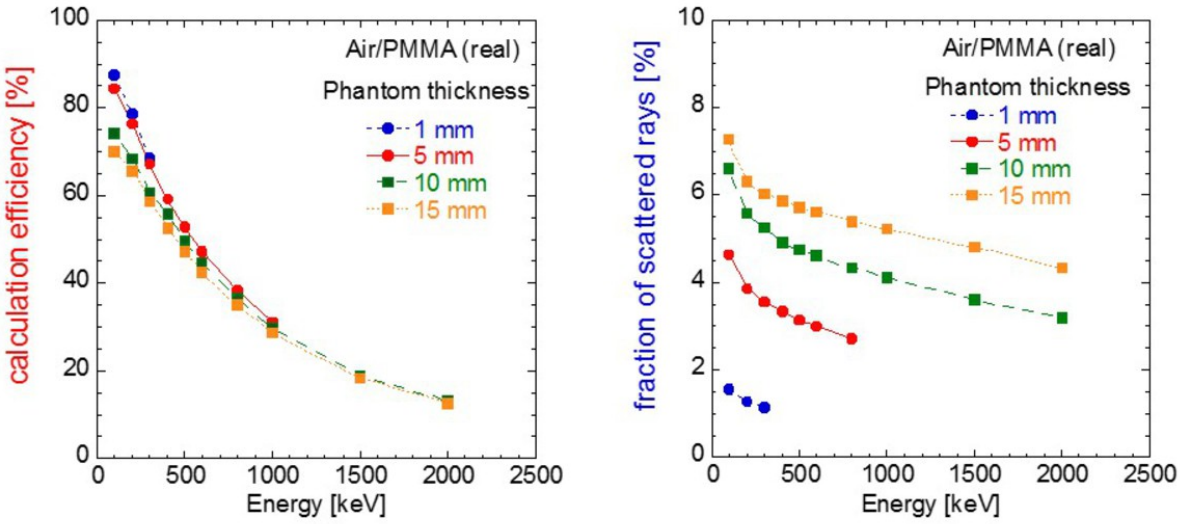

Fig. 9: Result of efficiency of Monte-Carlo simulation and fraction of scattered rays.

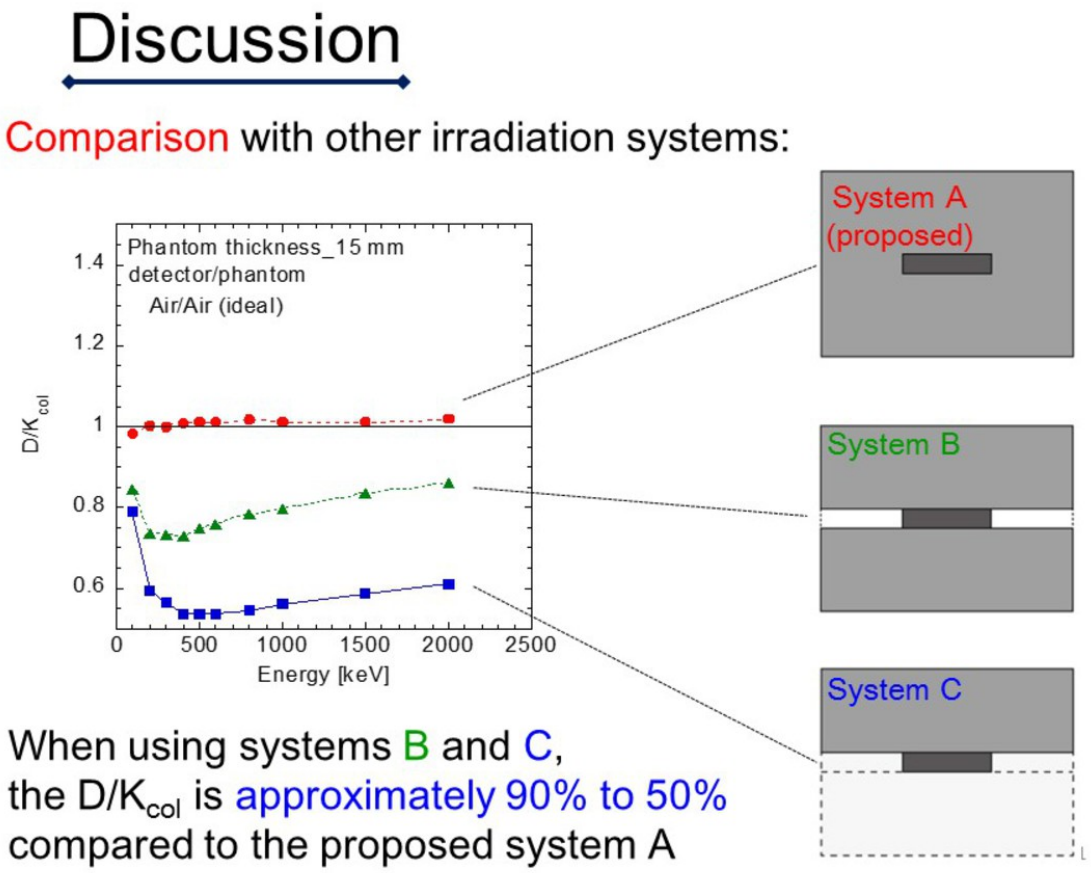

Fig. 10: Demonstration to indicate the purpose of our system. By comparing three different conditions, it was found that our system is most suitable for a compact irradiation system when considering secondary electron equilibrium.

Conclusion

In conclusion, we proposed a new irradiation system in order to evaluate the basic properties of the nanoDot OSL dosimeter in a simulation study. In the method, the detection region was totally covered with phantoms having thicknesses of 1-15 mm which enables the establishment of small irradiation fields. We evaluated the accuracy of our system by comparing an absorbed dose and collision kerma. As a result, we found that they agree with an accuracy of 10%. The calculation efficiency was greatly improved. The fractions of scattered rays were evaluated to be at most 5%. From these results, we evaluated that the accuracy of our system is approximately 10%. We plan to measure the efficiency of the nanoDot OSL dosimeter based on the present research as represented in **Fig. 11**.

Images for this section:

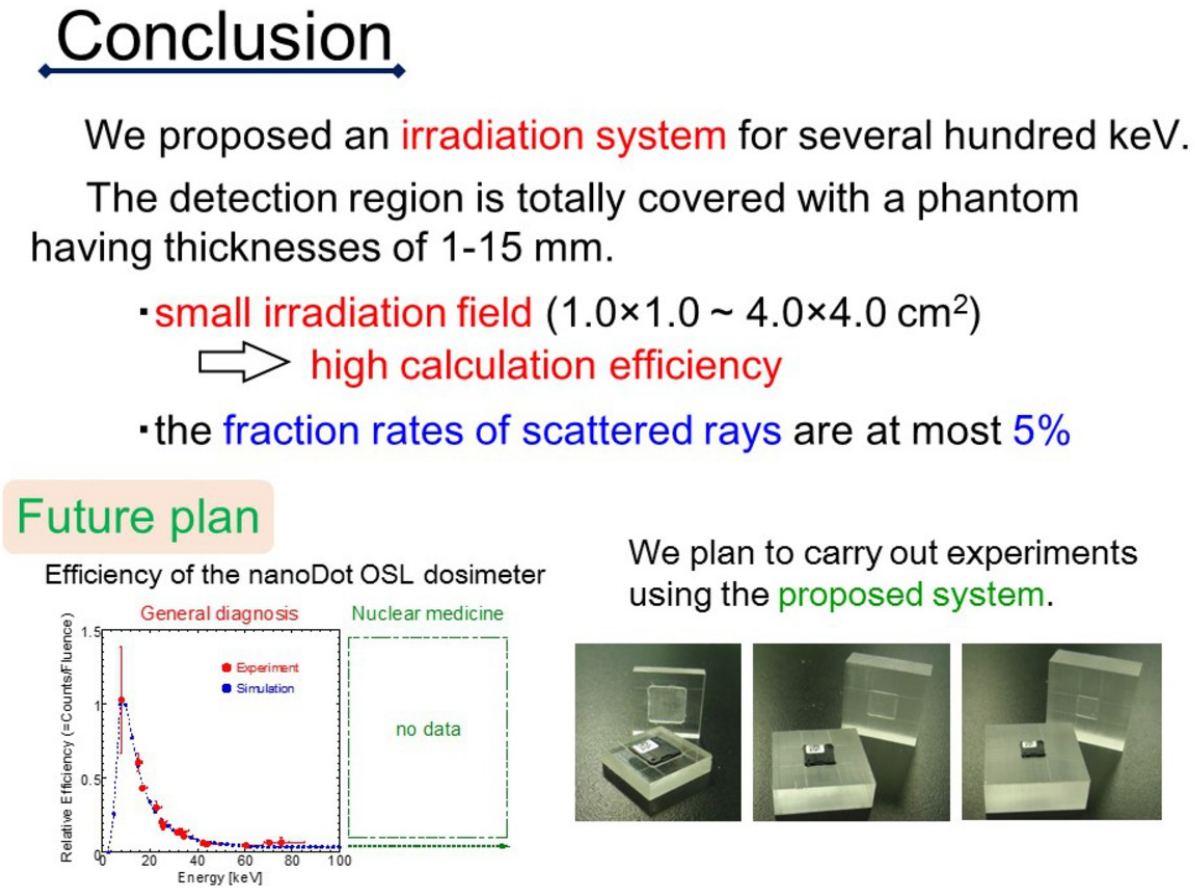

Fig. 11: Conclusion of our study and future plans.

Personal information

Hiroki Okino

Graduate School of Health Sciences, Tokushima University, Japan

References

[1] Grosswendt B: Backscatter factors for x-rays generated at voltages between 10 and 100 keV, Physics in Medical and Biology 29(5), 579-591, 1984.

[2] Klevenhagen SC: Experimentally determined backscatter factors for x-rays generated at voltages between 16 and 140 kV, Physics in Medical and Biology 34(12), 1871-1882, 1989.

[3] Grosswendt B: Dependences of the photon backscatter factor for water on source-to-phantom distance and irradiation field size, Physics in Medical and Biology 35(9), 1233-1245, 1990.

[4] Jursinic PA: Characterization of optically stimulated luminescent dosimeters, OSLDs, for clinical dosimetric measurements, Medical Physics 34(12), 4594-4604, 2007.

[5] Reft CS: The energy dependence and dose response of a commercial optically stimulated luminescent detector for kilovoltage photon, megavoltage photon, and electron, proton, and carbon beams, Medical Physics 36(5), 1690-1699, 2009.

[6] Lehmann J, Dunn L, Lye JE *et al*.: Angular dependence of the response of the nanoDot OSLD system for measurements at depth in clinical megavoltage beams. Medial Physics 41(6), 061712-1-9, 2014.

[7] Kerns JR, Kry SF, Sahoo N *et al*.: Angular dependence of the nanoDot OSL dosimeter, Medical Physics 38(7), 3955-3962, 2011.

[8] Al-Senan RM and Hatab MR: Characteristics of an OSLD in the diagnostic energy range, Medical Physics 38(7), 4396-4405, 2011.

[9] Hayashi H, Nakagawa K, Okino H, Takegami K, Okazaki T, Kobayashi I. High accuracy measurements by consecutive readings of OSL dosimeter. Medical Imaging and Information Sciences. 2014;31(2):28-34.

[10] Nakagawa K, Hayashi H, Okino H, Takegami K, Okazaki T, Kobayashi I. Fabrication of Annealing Equipment for Optically Stimulated Luminescence (OSL) Dosimeter. Japanese Journal of Radiological Technology. 2014;70(10):1135-1142 (in Japanese).

[11] Hayashi H, Takegami K, Okino H, Nakagawa K, Okazaki T, Kobayashi I. Procedure to measure angular dependences of personal dosimeters by means of diagnostic X-ray equipment. Medical Imaging and Information Sciences. 32(1), 8-14, 2015.

[12] Okazaki T, Hayashi H, Takegami K, Okino H, Nakagawa K. Evaluation of angular dependence of nanoDot OSL dosimeters toward direct measurement of entrance skin dose. European Congress of Radiology (EPOS). 2015; DOI: 10.1594/ecr2015/C-0721.

[13] Takegami K, Hayashi H, Okino H, Kimoto N, Maehata I, Kanazawa Y, Tohru O, Kobayashi I. Practical calibration curve of small-type optically stimulated luminescence (OSL) dosimeter for evaluation of entrance-skin dose in the diagnostic X-ray. Radiological Physics and Technology. 2015.

[14] Takegami K, Hayashi H, Nakagawa K, Okino H, Okazaki T, Kobayashi I. Measurement method of an exposed dose using the nanoDot dosimeter. European Congress of Radiology (EPOS). 2015; DOI:10.1594/ecr2015/C-0218.

[15] H. Hirayama et al. The EGS5 Code System. SLAC Report number: SLAC-R-730. KEK Report number: 2005-8., 2013.

[16] EGS5 community HP in KEK, http://rcwww.kek.jp/egsconf/

[17] L. Pages, E. Bertel, H. Joffre, et al., Energy Loss, Range, and Bremsstrahlung Yield for 10-kev to 100MeV Electrons in Various Elements and Chemical Compounds, Atomic Data and Nuclear Data Tables 4, 1-127. 1972.

[18] T. E. Johnson, B. K. Birky, Health Physics and Radiological Health, Lippincott Williams & Wilkins, 2012.

[19] R. Beherens, M. Kowatari and O. Hupe. Secondary Charged Equilibrium in 137Cs and 60Co Reference Radiation Fields. Radiation Protection Dosimetry, Vol. 136, 168-175, 2009.